



Cite this: DOI: 10.1039/c8ay02486c

Concentration-dependent multicolor fluorescent carbon dots for colorimetric and fluorescent bimodal detections of Fe³⁺ and L-ascorbic acid†

Lihong Shi,^{ID}* Zhipeng Hou, Caihong Zhang, Guomei Zhang, Yan Zhang,^{ID}
Chuan Dong^{ID} and Shaomin Shuang^{ID}*

We present a green and facile strategy for fabrication of concentration-dependent multicolor fluorescent carbon dots (CDs) by using coffee, salvia, and urea as the starting material *via* a one-step hydrothermal method. The obtained CDs emit three different colors of fluorescence (*i.e.* orange, yellow, and blue) with their concentration reduction. Moreover, yellow fluorescent CDs (Y-CDs) are utilized as a platform for colorimetric and fluorescent dual-mode detections of Fe³⁺ and L-ascorbic acid (L-AA) with high selectivity and sensitivity. The fluorescence of Y-CDs can be effectively quenched by Fe³⁺ based on static quenching and subsequently recovered upon the addition of L-AA due to the competitive complexation of L-AA with Fe³⁺. Therefore, the as-prepared Y-CDs could serve as a highly efficient fluorescent probe for “on–off–on” sequential determination of Fe³⁺ and L-AA. It is more attractive that Fe³⁺ and L-AA can also be visualized by this nanosensor *via* evident color changes under daylight. Furthermore, the designed nanosensor can be extended to detect intracellular Fe³⁺ and L-AA with outstanding biocompatibility and cellular imaging capability, which holds great promise in biomedical applications.

Received 14th November 2018
Accepted 23rd December 2018

DOI: 10.1039/c8ay02486c

rsc.li/methods

1. Introduction

As a rising star in the carbon nanomaterial family, carbon dots (CDs) have generated intense attention by virtue of their high photostability, superior biocompatibility, low toxicity, and excellent optical properties.^{1–5} In particular, the multicolor emission endows CDs with numerous exciting applications, such as bioimaging,^{6–10} chemical sensing,^{11,12} solid state lighting,^{13–15} medical diagnosis,¹⁶ and fingerprint detection.¹⁷ During the past few years, multicolor fluorescent CDs have been successfully synthesized by tuning various parameters, including particle size, excitation wavelength, and carbon source. Bao *et al.*⁶ obtained CDs with various colors of fluorescence through varying their size by ultrafiltration. Nie *et al.*⁷ synthesized excitation-dependent full-color emissions CDs by changing the reaction conditions of chloroform and diethylamine. The unique emission characteristics were ascribed to the surface functional groups which efficiently introduce new energy levels for electron transitions. Jiang *et al.*¹⁸ prepared three color CDs, *i.e.* blue, green, and red emissions, by thermal treatment using ethanol solution of *p*-phenylenediamine, *o*-phenylenediamine, and *m*-phenylenediamine, respectively, and

attributed the observed photoluminescence (PL) red shift to the difference in the nitrogen content of the CDs and their particle size.

Regardless of these opinions, an interesting fact has been discovered that the luminescence of CDs can be tuned by changing the concentration and accordingly the intermolecular interaction as well as the surface electron distribution. Meng *et al.*¹⁹ produced CDs by the reaction of coal pitch powder with a mixed solution of formic acid and H₂O₂ without any external heating and tuned fluorescence emission wavelengths from 630 to 400 nm by changing the concentration of CDs. Chen *et al.*²⁰ used citrate acid and ethanolamine as precursors to synthesize CDs with different colors in DMF and an aqueous solution as the concentration changed, which is due to the existence of multi-emissive centers in CDs from the core state, the edge state and surface states, and the polarity of the solution. Wang *et al.*¹¹ used a facile hydrothermal treatment of the mixed solution of *m*-phenylenediamine, ethanol, and ammonia to fabricate CDs with three strongest PL peaks with concentration reduction. Nevertheless, all these methods use toxic/expensive solvents or starting materials. Natural materials-derived concentration-dependent multicolor fluorescent CDs are very rare. Therefore, the development of the green synthesis of concentration-tunable multicolor emission CDs is still highly desired.

Iron is an essential element of the human body, which can increase resistance to diseases, regulate tissue respiration, prevent fatigue, and constitute hemoglobin. Inadequate and

College of Chemistry and Chemical Engineering, Shanxi University, Taiyuan 030006, PR China. E-mail: shilihong@sxu.edu.cn; smshuang@sxu.edu.cn

† Electronic supplementary information (ESI) available. See DOI: 10.1039/c8ay02486c

excessive iron intake can disturb the cellular homeostasis and induce various biological disorders.^{21,22} Thus, the reliable detection of Fe³⁺ has become indispensable from the viewpoint of human health. Current detection assays include voltammetry, spectrophotometry,^{23,24} atomic absorption spectrometry,²⁵ and inductively coupled plasma mass spectrometry (ICP-MS).²⁶ However, all these methods suffer from some drawbacks like the requirement of sophisticated instrumentation and tedious sample preparation procedures, limiting their practical applications.² The fluorescence-based Fe³⁺ probe becomes a good alternative due to its simple operation, high sensitivity, cost effectiveness, and rapid response. Also, colorimetry is an important method of detection which allows a direct analysis of the substrate simply by the naked eye. However, the detection of Fe³⁺ based on CDs by both fluorescence and colorimetry has not been reported yet. In addition, L-ascorbic acid (L-AA) is an important reducer, which has been used for the prevention and treatment of vitiligo, cancer, and scurvy.²⁷ Hence, the measurement of the L-AA level in solution and biological systems is necessary. Although miscellaneous strategies have been introduced for the quantitative detection of L-AA, many endeavors are still continuously being made to search for better strategies to detect the content of L-AA in biological samples.

In this paper, concentration-dependent multicolor fluorescent CDs have been prepared by hydrothermal treatment of coffee, salvia, and urea. The as-synthesized CDs show orange, yellow, and blue fluorescence with their concentration reduction. Yellow fluorescent CDs (Y-CDs) are utilized for fluorescent and colorimetric detection of Fe³⁺ and L-AA sequentially. In addition, Y-CDs could image the fluctuation of Fe³⁺ and L-AA in living cells with appreciable changes in fluorescence.

2. Experimental

2.1 Materials

AlCl₃, BaCl₂, BiCl₃, CaCl₂, CdCl₂, CuCl₂, FeCl₃, HgCl₂, KCl, MgCl₂, MnCl₂, NaCl, NiCl₂, and ZnCl₂ were purchased from Beijing Chemical Corp (Beijing, China). Coffee and salvia were purchased from a local market (Taiyuan, China). And urea was purchased from Sigma Aldrich Trade Co., Ltd (Shanghai, China). Distilled deionized (DDI) water was obtained from a Millipore Milli-Q-RO4 water purification system with a resistivity higher than 18 MΩ cm⁻¹ (Bedford, MA, USA). Dialysis membranes with a MWCO of 500–1000 Da were purchased from Beijing Solarbio Science & Technology Co., Ltd. (Beijing, China). Human hepatoma cellular carcinoma (SMMC-7721) cells were purchased from the Taiyuan Armed Police Hospital (Taiyuan, China).

2.2 Synthesis of CDs

The CDs were prepared by hydrothermal treatment of coffee, salvia and urea. 0.5 g coffee, 0.5 g salvia, and 0.2 g urea were dissolved in 20 mL DDI water. Then the cloudy solution was poured into a 50 mL hydrothermal reactor vessel, placed in an oven, and heated at 220 °C for 5 h. After cooling down to room temperature, the CDs were collected by removing larger particles through centrifugation at 4000 rpm for 20 min and then

dialyzed through a dialysis membrane with MWCO of 500–1000 Da for 24 h.

2.3 Characterization

The transmission electron microscopy (TEM) study was carried out using a JEOL JEM-2100 instrument operating at an accelerating voltage of 200 kV. Samples for TEM measurements were prepared by placing a drop of colloidal solution on a carbon-coated copper grid and then dried at room temperature. The UV-vis absorption spectrum of CDs was recorded using a HITACHI U-2910 UV. Fluorescence spectra were recorded with a Hitachi F-4500 fluorescence spectrophotometer. The Fourier transform infrared (FTIR) spectrum was recorded on a Bruker tensor 2 spectrometer using a resolution of 4 cm⁻¹. The sample with 1 mg diluted with KBr (ratio 1 : 200) was pressed into discs. Atomic force microscope (AFM) images were obtained using an AFM Bruker MultiMode 8 in the contact mode. The fluorescence lifetime was measured using an Edinburgh FLS920.

2.4 Fluorimetry for the determination of Fe³⁺ and L-AA

The detection of Fe³⁺ was performed at room temperature in Tris-HCl buffer (pH = 7.4). In a typical run, a 0.1 mL CD dispersion was added to 0.233 mL Tris-HCl buffer at 38.4 mg L⁻¹ final concentration, followed by the addition of Fe³⁺ standard with various concentrations. The fluorescence emission spectra were recorded after reaction for 1 min at room temperature.

The effect of L-AA on the fluorescence intensity of the Y-CDs/Fe³⁺ solution mixture was conducted as follows. The L-AA standard with various concentrations was added to the Y-CDs (38.4 mg L⁻¹)/Fe³⁺ (400 μM) solution mixture. The fluorescence emission spectra were recorded after reaction for 1 min at room temperature.

2.5 Cellular imaging

Human hepatoma cellular carcinoma (SMMC-7721) cells were cultured in Dulbecco's Modified Eagle Medium (DMEM) supplemented with 10% FBS and incubated at 37 °C in a 5% CO₂ atmosphere. 0.0384 mg CDs were added to 1.0 mL culture medium at 38.4 mg L⁻¹ final concentration. After incubation for 24 h, the SMMC-7721 cells were harvested using 0.25% trypsin/0.020% EDTA, washed three times (1.0 mL each) with pH 7.4 Tris-HCl. Y-CD-stained SMMC-7721 cells were treated with Fe³⁺ with a concentration of 400 μM for 2 min. After that, the cells were treated with L-AA (57.14 mM) for 3 min.

All fluorescence images were collected with a Zeiss LSM 880 confocal laser-scanning microscope. The cell images were taken at a λ_{ex}/λ_{em} of 405/435–450, 488/492–577 and 514/620–700 nm, respectively.

3. Results and discussion

3.1 The synthesis of multicolor fluorescent CDs

The successful fabrication of concentration-dependent multicolor fluorescent CDs was carried out by using coffee, salvia, and urea as the starting material *via* a one-step hydrothermal

method (Fig. 1). For this one-step approach, the most favorable feature is that the formation of carbon dots and its surface passivation can be realized simultaneously.⁸ We use inexpensive coffee as well as salvia as the carbon source and urea as a surface passivation agent. CD formation by a hydrothermal method may involve dehydration, polymerization, pyrolysis, and surface passivation processes in a closed system under self-generated pressure and at mild temperature.

3.2 PL properties of the CDs

PL properties of the as-prepared CDs depend on the concentration as well as excitation wavelengths.¹¹ Fig. 2 shows the PL spectra of CD solution with a concentration of 128, 38.4, and 2.56 mg L⁻¹. The strongest emission peaks of these three samples are around 616, 550, and 436 nm and accordingly the corresponding samples are named O-, Y-, and B-CDs, respectively. The O-CDs exhibit excitation-independent emission while Y- and B-CDs exhibit excitation-dependent emission. Particularly, these three strongest PL peaks barely shift when the concentrations of O-, Y-, and B-CDs are varied in 76.8–128, 38.4–64 and 2.56–12.8 mg L⁻¹. The concentration-dependent properties of CDs could be attributed to their interactions similar to intermolecular forces.²⁰ The surface state of CDs is a predominant factor for the fluorescence emission process. The energy gap of the surface states, where electrons and holes recombine to emit fluorescence, correlates closely with the extent of the π -electron system and surface chemistry. The surface states of CDs are regulated by carbonyl, hydroxy,

aromatic structures, amino, and C=C bonds. As the concentration decreases, the intermolecular forces pull the CDs closer together, and the functional groups on the surface of CDs combine to reduce the energy gap, which ultimately leads to a red shift of excitation/emission maxima.^{28–30} The photographs of O-, Y-, and B-CDs under daylight and the indicated wavelength excitation are shown in the insets of Fig. 2A–C. Taking into account fluorescence color and fluorescence intensity, we finally chose Y-CDs for detection and imaging.

3.3 The characterization of the CDs

The size distribution and morphology of CDs were assessed by TEM. As shown in Fig. 3A–C, CDs are spherical and well dispersed. Based on the statistical analysis of above three hundred particles, the mean diameter is about 2.94 ± 0.04 nm (the inset of Fig. 3A) and about 88% of CDs fall within the range from 2.25 nm to 4.75 nm. The high resolution TEM (HRTEM) image (Fig. 3D) shows that CDs possess a crystalline structure with a lattice spacing of 0.21 nm, being attributed to the (100) facet of graphite. This result strongly suggests that the synthesized CDs exhibit a graphite-like structure.³¹

The AFM images (Fig. S1†) show the surface morphology of the as-prepared CDs. The AFM topography image (Fig. S1A†) and three-dimensional image (Fig. S1B†) clearly show that CDs have good dispersivity. Fig. S1C† is a radial height distribution map along the line in the AFM topography image. As shown in Fig. S1D,† the height of CDs is from 1.5 nm to 2.3 nm with a mean height of *ca.* 1.92 nm. This is consistent with TEM data.

We used FTIR to identify the functional groups of CDs (Fig. S2A†). In the FTIR spectrum of CDs, the peak at 3194 cm⁻¹ represents the O–H stretching vibrations, the peak at 1658 cm⁻¹ shows the C–O bending vibrations, the peak at 1654 cm⁻¹ corresponds to the C–N stretching vibrations and N–H bending vibrations, the peaks at 1477, 1383, 756, and 690 cm⁻¹ are associated with the C–H bending vibrations, and the peaks at 1232 and 1068 cm⁻¹ suggest the existence of the C–O–C stretching vibrations. Additionally, the PL intensity of CDs remains almost constant even after excitation for 50 min (Fig. S2B†), suggesting that the photostability of CDs is eminent. The PL intensities stay almost stable when the pH value was changed from 7.0 to 9.2 (Fig. S2C†), which shows that the PL intensity of CDs is pH independent.



Fig. 1 Diagram for the fabrication of concentration-dependent multicolor fluorescent CDs.

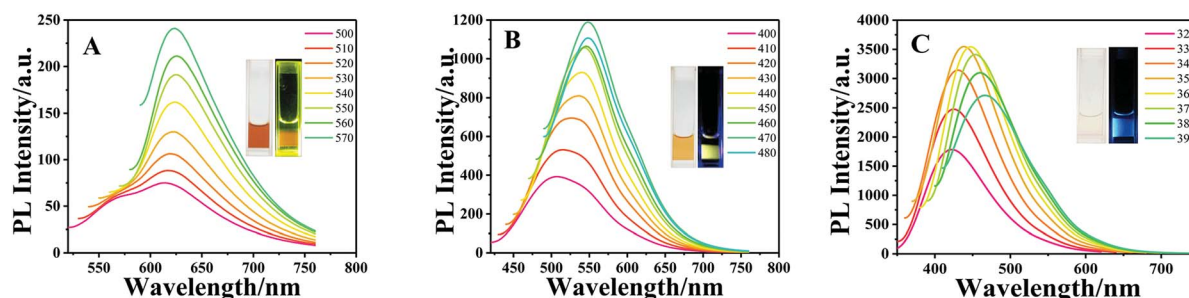


Fig. 2 PL spectra of CDs with different concentrations (A) 128 mg L⁻¹, (B) 38.4 mg L⁻¹, and (C) 2.56 mg L⁻¹ at different excitation wavelengths. Inset: photographs of the corresponding samples under daylight and indicated wavelength excitation.

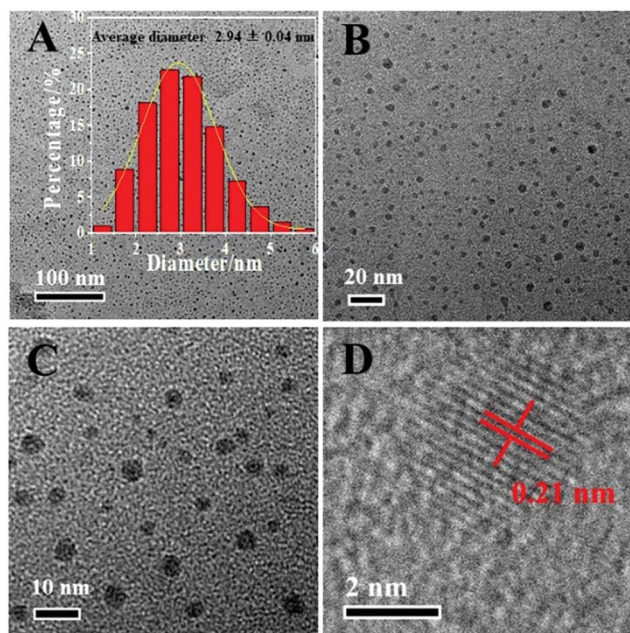


Fig. 3 TEM images of CDs: (A) scale bar is 100 nm (inset: size distribution of CDs), (B) scale bar is 20 nm, and (C) scale bar is 10 nm. (D) HRTEM image of CDs, scale bar is 2 nm.

3.4 Fe³⁺ and L-AA sensing of Y-CDs in aqueous solution

The influence of 14 kinds of metal ions on the PL intensity of Y-CDs under pH 7.4 conditions was studied, including Cd²⁺, Cu²⁺, Ca²⁺, Fe³⁺, Hg²⁺, Ba²⁺, Bi³⁺, Ni²⁺, Mg²⁺, Zn²⁺, Mn²⁺, K⁺, Al³⁺, and Na⁺ (Fig. 4A). Among these metal ions, Fe³⁺ exhibits the largest quenching of the fluorescence of the Y-CDs while other metal ions do not have a significant effect on the fluorescence intensity of Y-CDs. Moreover, no obvious interference is observed even with high concentrations (up to 400 μM) of other metal ions. In comparison with other ions, the high selectivity of Y-CDs for Fe³⁺ may be attributed to the faster coordination of Fe³⁺ ions with the N containing functional groups in Y-CDs.³² Therefore, the Y-CDs have high selectivity toward Fe³⁺ over the other metal ions and could be designed as an efficient “turn-off” fluorescence Fe³⁺ sensor. Also, we investigated the Fe³⁺ sensing capacity of Y-CDs in the range of 0 μM to 400 μM (Fig. 4B). The fluorescence intensity at 548 nm decreases progressively as the Fe³⁺ concentration increases. Meanwhile, the photographs of a Y-CD solution under 470 nm excitation were taken (the inset of Fig. 4B) which display that the fluorescence color of Y-CD solution changes from yellow to colorless with the increase of Fe³⁺ concentration. Fig. 4C presents PL data *versus* the concentration of Fe³⁺. There is a good linearity between the F/F_0 and Fe³⁺ concentration in the range of 0.5–175 μM and 200–400 μM, respectively. The corresponding regression coefficient (R^2) is 0.99704 and 0.98621, respectively. The detection limit of 27.8 nM is obtained based on a signal-to-noise ratio of 3, showing lower value than those previously reported for the Fe³⁺ detection (Table S1†). The results show that the sensor is highly sensitive and has a wide linear range. To further investigate the PL quenching mechanism, UV-vis absorption experiments on

the Y-CDs at various concentrations of Fe³⁺ were performed (Fig. 4D). The absorption changes constantly with increasing Fe³⁺ concentrations, implying that fluorescence quenching can be attributed to static quenching arising from the formation of a stable non-fluorescent complex between CDs and Fe³⁺.^{3,22,33} In addition, the fluorescence lifetime is also effective evidence to distinguish the quenching type. Thus, fluorescence emission decay curves of Y-CDs in the absence and presence of Fe³⁺ were measured (Fig. S3†). The lifetimes of Y-CDs and Y-CDs/Fe³⁺ are calculated to be 5.27 ns and 5.45 ns (Table S2†), which proves that the fluorescence quenching of Y-CDs in the presence of Fe³⁺ is a static quenching process on account of the formation of the Y-CDs/Fe³⁺ complex. The consequence of the fluorescence lifetime is in accord with that of UV-vis absorption spectra.

The colorimetric sensing behavior of Y-CDs was investigated by monitoring color changes upon addition of different metal ions. The addition of Fe³⁺ to Y-CD solution results in an apparent color change from pale yellow to dark-brown (Fig. 4E), while other metals cause no change in color. The color change of the solution may also stem from the complex interaction between CDs and Fe³⁺.³⁴ Thus, we can also use colorimetric methods to identify Fe³⁺. Fe³⁺ ions are transition metals and contain an unfilled d orbital. When CDs coordinate with Fe³⁺, electrons on the CDs are more likely to enter the unfilled d orbital of Fe³⁺, and charge transfer occurs, causing gradual deepening of the solution color. Fig. 4F shows the color change after adding different concentrations of Fe³⁺ under daylight. It can be seen that as the concentration of Fe³⁺ increases, the color of Y-CD solution continually changes from pale yellow to dark-brown. These results demonstrate that the Y-CDs are an intuitive and convenient potential naked-eye sensor for Fe³⁺.

At the same time, it is exciting that we have found that the addition of L-AA could recover the fluorescence of Y-CDs quenched by Fe³⁺. We studied the influence of various external substances on the PL intensity of the Y-CDs/Fe³⁺ under pH 7.4 conditions, including cations, anions, small molecules, and amino acids (Fig. S4†). Among these substances, L-AA exhibits the largest recovery of the fluorescence of Y-CDs/Fe³⁺, while other substances have a slight effect. Meanwhile, the interference experiment of Y-CDs/Fe³⁺ was also implemented (Fig. S4†), showing that these substances have no effect on the recovery of fluorescence. These results demonstrate that Y-CDs/Fe³⁺ has good selectivity and strong anti-interference ability for L-AA sensing.

Therefore, the Y-CDs/Fe³⁺ system could be developed as an “off-on” fluorescence probe for detection of L-AA. As illustrated in the proposed “on-off-on” sensing process (Fig. 5), the colors of Y-CDs, Y-CDs/Fe³⁺, and Y-CDs/Fe³⁺/L-AA solution vary under irradiation with daylight and 470 nm excitation. The fluorescence intensity at 548 nm is gradually recovered with increasing concentrations of L-AA (Fig. 6A) Meanwhile, the photographs of Y-CDs/Fe³⁺ solution under 470 nm excitation were taken (the inset of Fig. 6A). Fig. 6B presents the fluorescence data *versus* the concentration of L-AA. In a good range of 3.23–22.08 mM and 33.33–57.14 mM, respectively, the corresponding regression coefficient (R^2) is 0.99645 and 0.99182, respectively. The

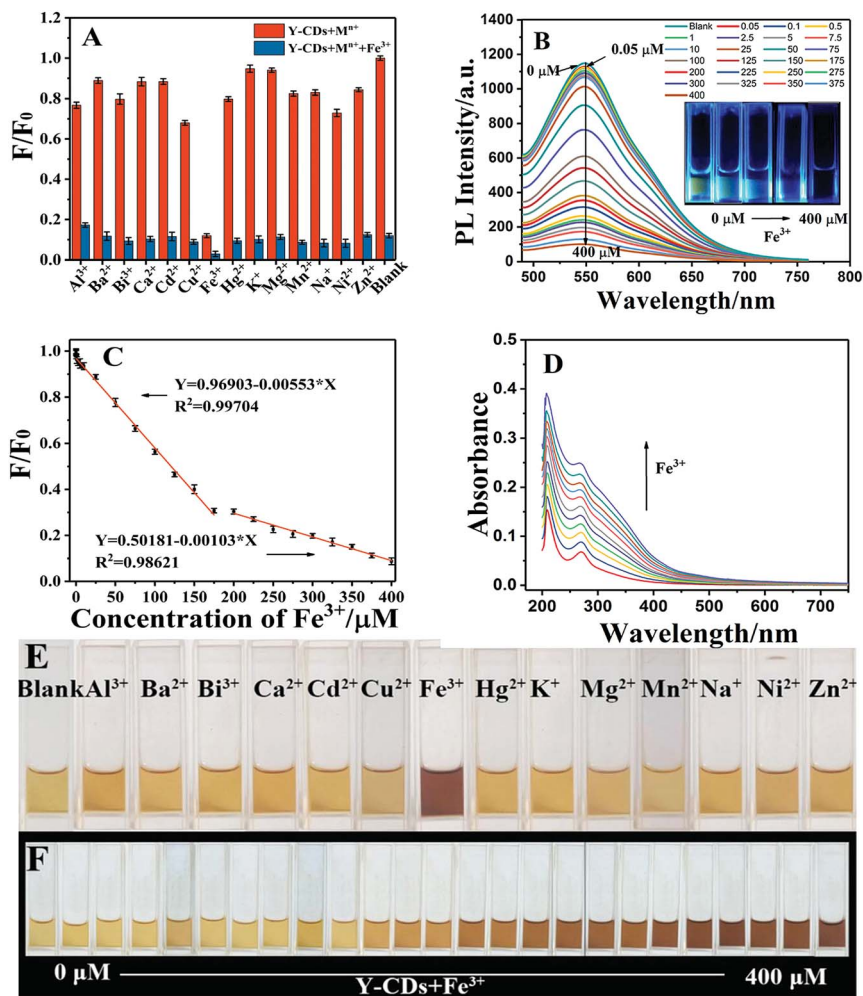


Fig. 4 (A) Selectivity of Y-CD solution for Fe³⁺ over other cations under pH 7.4 conditions at 470 nm excitation. The red bars represent the addition of metal ions (400 μM for all the metal ions) to Y-CD solution. The blue bars represent the subsequent addition of 400 μM Fe³⁺ to Y-CD solution. (F_0 and F are the fluorescence intensity of Y-CDs in the absence and presence of external ions, respectively). (B) Representative fluorescence emission spectra of Y-CDs in the presence of various concentrations of Fe³⁺ (0–400 μM). (C) The relationship between the F/F_0 and Fe³⁺ concentration from 0 μM to 400 μM. The linear relationship between the fluorescence intensity and Fe³⁺ concentration in the ranges of 0.5–175 μM and 200–400 μM. (D) UV-vis absorption spectra of Y-CDs in the presence of various concentrations of Fe³⁺. (E) The color changes of Y-CD solution to different cations (400 μM) under daylight. (F) The color changes of Y-CD solution to various concentrations of Fe³⁺ (0–400 μM) under daylight.

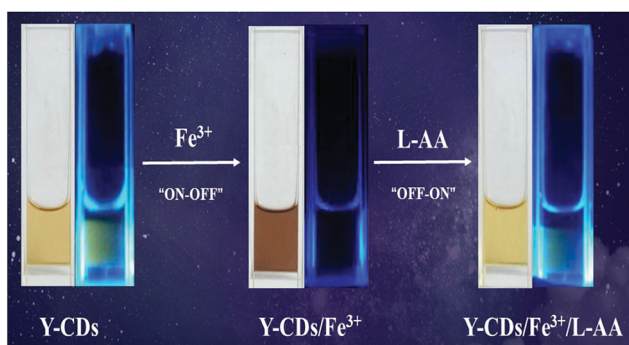


Fig. 5 Photographs of Y-CDs in the absence of Fe³⁺ and L-AA (first), in the presence of Fe³⁺ (second), and in the presence of Fe³⁺ and L-AA (third) under daylight and 470 nm excitation.

detection limit was calculated to be 1.8 mM for L-AA based on a signal-to-noise ratio of 3. Compared with previous work (Table S3[†]), the proposed L-AA probe is more selective and less sensitive. The fluorescence recovery of Y-CDs/Fe³⁺ by L-AA is likely due to the following reasons. First, the fluorescence recovery of Y-CDs/Fe³⁺ solution is actually attributable to the stronger binding affinity of L-AA towards Fe³⁺, which removes Fe³⁺ from the surface of Y-CDs. Second, for the Y-CDs/Fe³⁺ system, Fe³⁺ oxidizes L-AA to diketogulonic acid and is reduced to Fe²⁺ simultaneously. The complex of diketogulonic acid with Fe²⁺ has strong absorption peak at 269 nm (Fig. 6C). At the same time, the color of the system changed from dark-brown to pale yellow under daylight with the increase of L-AA concentrations (Fig. 6D). These results also demonstrate that Y-CDs/Fe³⁺ is a potential naked-eye sensor for L-AA.

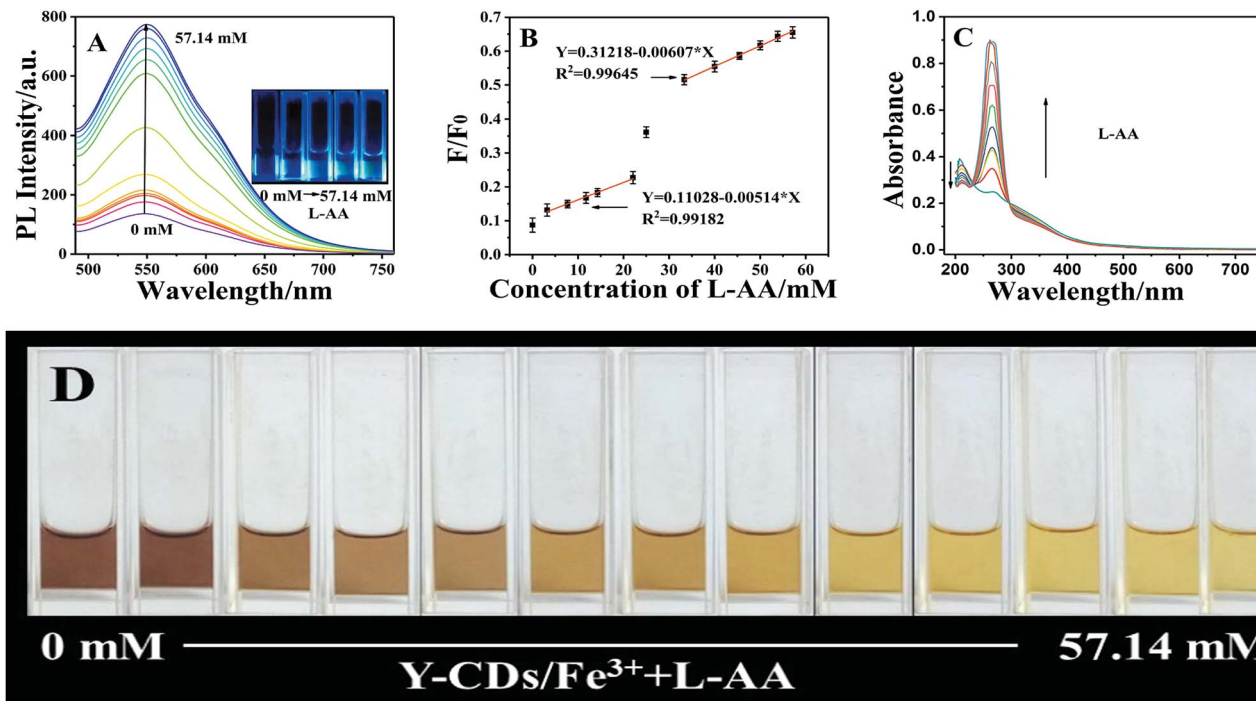


Fig. 6 (A) Representative fluorescence emission spectra of Y-CDs/Fe³⁺ in the presence of various concentrations of L-AA (0–57.14 mM). (B) The relationship between the F/F_0 and L-AA concentration from 0 to 57.14 mM. The linear relationship between the fluorescence intensity and L-AA concentration in the ranges of 3.23–22.08 mM and 33.33–57.14 mM. (F_0 is the fluorescence intensity of Y-CDs in the absence of Fe³⁺ and L-AA and F is the fluorescence intensity of Y-CDs/Fe³⁺ in the presence of L-AA.) (C) UV-vis absorption spectra of Y-CDs/Fe³⁺ in the presence of various concentrations of L-AA. (D) The color changes of Y-CDs/Fe³⁺ solution to various concentrations of L-AA (0–57.14 mM) under daylight.

3.5 Cell cytotoxicity assay

To explore the potential application of CDs in live cell imaging, it is required that the selected fluorescent marker possesses not only optical merits but also low cytotoxicity.³⁵ To evaluate the cytotoxicity of the as-prepared CDs, we performed the MTT assay in SMMC-7721 cells with concentrations ranging from

10 mg L⁻¹ to 50 mg L⁻¹. The results demonstrate that more than 86.5% of the cells are viable (Fig. S5[†]), which implies the low toxicity of Y-CDs to cultured cells under the experimental conditions at a concentration of 38.4 mg L⁻¹. The Y-CDs were internalized into the cells possibly by an endocytosis mechanism.³⁶

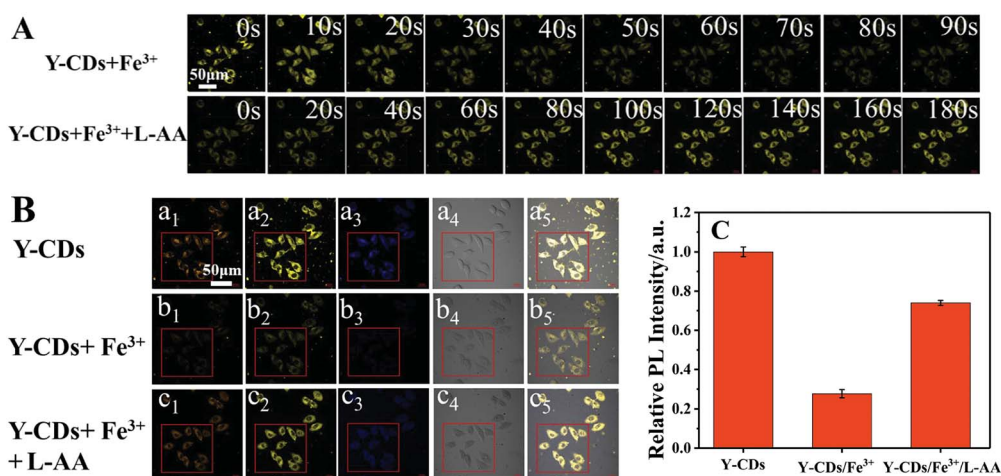


Fig. 7 (A) Dynamic LSCM fluorescence imaging of SMMC-7721 cells with Y-CDs/Fe³⁺ and Y-CDs/Fe³⁺/L-AA ($\lambda_{ex}/\lambda_{em}$: 488 nm/492–577 nm). (B) LSCM images of SMMC-7721 cells incubated with Y-CDs, Y-CDs/Fe³⁺ (400 μM), and Y-CDs/Fe³⁺ (400 μM)/L-AA (57.14 mM). The first, second, and third panels are cell images taken at a $\lambda_{ex}/\lambda_{em}$ of 405 nm/435–450 nm, 488 nm/492–577 nm, and 514 nm/600–700 nm, respectively. The fourth panel shows the bright field images. The fifth panel is the merged image of the first, second, third and fourth panels. (C) Intracellular fluorescence responses of Y-CDs, Y-CDs/Fe³⁺ (400 μM), and Y-CDs/Fe³⁺ (400 μM)/L-AA (57.14 mM). Data are expressed as mean \pm standard deviation. The intensities of 10 cells are measured. Scale bar is 50 μm.

3.6 *In vitro* cellular imaging determination of Fe³⁺ and L-AA

We used SMMC-7721 cells as a model to study the Fe³⁺ and L-AA dependent fluorescence imaging of Y-CDs using a laser scanning confocal microscope (LSCM). SMMC-7721 cells were labelled with Y-CDs. As depicted in Fig. 7A, when Fe³⁺ entered Y-CD-stained SMMC-7721 cells, the yellow fluorescence was gradually weakened and can hardly be seen after 90 s.

Sequentially, when L-AA was added the yellow emission was progressively recovered in 180 s, indicating that the emission of Y-CDs/Fe³⁺ in the cells can be recovered by L-AA. Fig. 7B shows the morphology of cells cultured in the three cases of Y-CDs, Y-CDs/Fe³⁺, and Y-CDs/Fe³⁺/L-AA. These cells emit orange (first panels in Fig. 7B), yellow (second panels in Fig. 7B), and blue (third panels in Fig. 7B) fluorescence when excited by 405, 488, and 514 nm lasers, respectively. The cells cultured with Y-CDs and Y-CDs/Fe³⁺/L-AA emit stronger fluorescence than those cultured with Y-CDs/Fe³⁺. The whole process shows that CDs have an excellent ability to label cells. Fig. 7C depicts the changes of the intracellular fluorescence intensities of Y-CDs without and with Fe³⁺ and L-AA, respectively. It is prominent that the emission intensities of the cells are in the order of Y-CDs > Y-CDs/Fe³⁺/L-AA > Y-CDs/Fe³⁺. The results illustrate that Y-CDs can be used as nanoprobe to “on–off–on” detect Fe³⁺ and L-AA in living cells.

4. Conclusion

We develop concentration-dependent orange–yellow–blue fluorescent CDs for colorimetric and fluorescent dual-mode detections of Fe³⁺ and L-AA. The concentration-dependent fluorescent CDs are prepared in a facile and eco-friendly manner by hydrothermal treatment of coffee, salvia, and urea. The as-prepared CDs exhibit low toxicity and excellent optical stabilities. The fluorescence intensity of Y-CDs is sensitive toward Fe³⁺ and L-AA, which are utilized as a nanoprobe for “on–off–on” determination of Fe³⁺ and L-AA. Meanwhile, a visible color change is observed during the determination of Fe³⁺ and L-AA. More importantly, Y-CDs could be successfully applied for imaging intracellular Fe³⁺ and L-AA. By the combination of fluorescent and colorimetric readouts, Y-CDs could be potentially used in water quality monitoring, medicine quality supervision, and biomedical controlling.

Conflicts of interest

There are no conflicts to declare.

Acknowledgements

This work was supported by the National Natural Science Foundation of China (21575084) and the Natural Science Foundation of Shanxi Province (201701D121019 and 201701D121017). We also acknowledge Dr Ying Zuo for her help with AFM measurements and Dr Juanjuan Wang for her help with Zeiss LSM 880 confocal laser-scanning microscope measurements from the Scientific Instrument Center at Shanxi University.

Notes and references

- 1 Y. Chen, Y. Wu, B. Weng, B. Wang and C. Li, *Sens. Actuators, B*, 2016, **223**, 689–696.
- 2 D. K. Dang, C. Sundaram, Y.-L. T. Ngo, J. S. Chung, E. J. Kim and S. H. Hur, *Sens. Actuators, B*, 2018, **255**, 3284–3291.
- 3 Y. Liu, Y. Liu, S.-J. Park, Y. Zhang, T. Kim, S. Chae, M. Park and H.-Y. Kim, *J. Mater. Chem. A*, 2015, **3**, 17747–17754.
- 4 X. Sun and Y. Lei, *Trends Anal. Chem.*, 2017, **89**, 163–180.
- 5 L. H. Shi, X. F. Li, Y. Y. Li, X. P. Wen, J. F. Li, M. M. F. Choi, C. Dong and S. M. Shuang, *Sens. Actuators, B*, 2015, **210**, 533–541.
- 6 L. Bao, C. Liu, Z. L. Zhang and D. W. Pang, *Adv. Mater.*, 2015, **27**, 1663–1667.
- 7 H. Nie, M. Li, Q. Li, S. Liang, Y. Tan, L. Sheng, W. Shi and S. X.-A. Zhang, *Chem. Mater.*, 2014, **26**, 3104–3112.
- 8 C. Liu, P. Zhang, F. Tian, W. Li, F. Li and W. Liu, *J. Mater. Chem.*, 2011, **21**, 13163.
- 9 H. Ding, S. B. Yu, J. S. Wei and H. M. Xiong, *ACS Nano*, 2016, **10**, 484–491.
- 10 L. H. Shi, B. Zhao, X. F. Li, G. M. Zhang, Y. Zhang, C. Dong and S. M. Shuang, *Sens. Actuators, B*, 2016, **235**, 316–324.
- 11 Y. Wang, Q. Chang and S. Hu, *Sens. Actuators, B*, 2017, **253**, 928–933.
- 12 C. Wang, T. Hu, Z. Wen, J. Zhou, X. Wang, Q. Wu and C. Wang, *J. Colloid Interface Sci.*, 2018, **521**, 33–41.
- 13 X. Guo, C. F. Wang, Z. Y. Yu, L. Chen and S. Chen, *Chem. Commun.*, 2012, **48**, 2692–2694.
- 14 L. H. Shi, L. Li, X. F. Li, G. M. Zhang, Y. Zhang, C. Dong and S. M. Shuang, *Sens. Actuators, B*, 2017, **251**, 234–241.
- 15 L. H. Shi, B. Zhao, X. F. Li, G. M. Zhang, Y. Zhang, C. Dong and S. M. Shuang, *Anal. Methods*, 2017, **9**, 2197–2204.
- 16 X. Wang, K. Qu, B. Xu, J. Ren and X. Qu, *Nano Res.*, 2011, **4**, 908–920.
- 17 J. Chen, J. S. Wei, P. Zhang, X. Q. Niu, W. Zhao, Z. Y. Zhu, H. Ding and H. M. Xiong, *ACS Appl. Mater. Interfaces*, 2017, **9**, 18429–18433.
- 18 K. Jiang, S. Sun, L. Zhang, Y. Lu, A. Wu, C. Cai and H. Lin, *Angew. Chem., Int. Ed.*, 2015, **54**, 5360–5363.
- 19 X. Meng, Q. Chang, C. Xue, J. Yang and S. Hu, *Chem. Commun.*, 2017, **53**, 3074–3077.
- 20 Y. Chen, H. Lian, Y. Wei, X. He, Y. Chen, B. Wang, Q. Zeng and J. Lin, *Nanoscale*, 2018, **10**, 6734–6743.
- 21 F. Du, X. Gong, W. Lu, Y. Liu, Y. Gao, S. Shuang, M. Xian and C. Dong, *Talanta*, 2018, **179**, 554–562.
- 22 C. Han, R. Wang, K. Wang, H. Xu, M. Sui, J. Li and K. Xu, *Biosens. Bioelectron.*, 2016, **83**, 229–236.
- 23 S. Lunvongsa, M. Oshima and S. Motomizu, *Talanta*, 2006, **68**, 969–973.
- 24 D. M. Gomes, M. A. Segundo, J. L. Lima and A. O. Rangel, *Talanta*, 2005, **66**, 703–711.
- 25 J. E. Andersen, *Analyst*, 2005, **130**, 385–390.
- 26 A. Matusch, C. Depboylu, C. Palm, B. Wu, G. U. Hoglinger, M. K. Schafer and J. S. Becker, *J. Am. Soc. Mass Spectrom.*, 2010, **21**, 161–171.
- 27 X. Gong, Z. Li, Q. Hu, R. Zhou, S. Shuang and C. Dong, *ACS Appl. Mater. Interfaces*, 2017, **9**, 38761–38772.

- 28 M. Hassan, V. G. Gomes, A. Dehghani and S. M. Ardekani, *Nano Res.*, 2017, **11**, 1–41.
- 29 H. Ding, S. B. Yu, J. S. Wei and H. M. Xiong, *ACS Nano*, 2016, **10**, 484–491.
- 30 Q. X. Mao, S. E, J. M. Xia, R. S. Song, Y. Shu, X. W. Chen and J. H. Wang, *Langmuir*, 2016, **32**, 12221–12229.
- 31 R. Atchudan, T. Edison, K. R. Aseer, S. Perumal, N. Karthik and Y. R. Lee, *Biosens. Bioelectron.*, 2018, **99**, 303–311.
- 32 S. Q. Liu, R. L. Liu, X. Xing, C. Q. Yang, Y. Xu and D. Q. Wu, *RSC Adv.*, 2016, **6**, 31884–31888.
- 33 R. Wang, X. Wang and Y. Sun, *Sens. Actuators, B*, 2017, **241**, 73–79.
- 34 Y. Liu, W. Duan, W. Song, J. Liu, C. Ren, J. Wu, D. Liu and H. Chen, *ACS Appl. Mater. Interfaces*, 2017, **9**, 12663–12672.
- 35 L. H. Shi, Y. Y. Li, X. F. Li, X. P. Wen, G. M. Zhang, J. Yang, C. Dong and S. M. Shuang, *Nanoscale*, 2015, **7**, 7394–7401.
- 36 L. H. Shi, Y. Y. Li, X. F. Li, B. Zhao, X. P. Wen, G. M. Zhang, C. Dong and S. M. Shuang, *Biosens. Bioelectron.*, 2016, **77**, 598–602.